Anisotropic diffusion limited aggregation in three dimensions: Universality and nonuniversality

Nicholas R. Goold,[1,*] Ellák Somfai,[1,2,†] and Robin C. Ball[1,‡]
[1]*Department of Physics, University of Warwick, Coventry CV4 7AL, United Kingdom*
[2]*Universiteit Leiden, Instituut-Lorentz, P. O. Box 9506, 2300 RA Leiden, The Netherlands*
(Received 28 January 2005; published 9 September 2005)

We explore the macroscopic consequences of lattice anisotropy for diffusion limited aggregation (DLA) in three dimensions. Simple cubic and bcc lattice growths are shown to approach universal asymptotic states in a coherent fashion, and the approach is accelerated by the use of noise reduction. These states are strikingly anisotropic dendrites with a rich hierarchy of structure. For growth on an fcc lattice, our data suggest at least two stable fixed points of anisotropy, one matching the bcc case. Hexagonal growths, favoring six planar and two polar directions, appear to approach a line of asymptotic states with continuously tunable polar anisotropy. The more planar of these growths visually resembles real snowflake morphologies. Our simulations use a new and dimension-independent implementation of the DLA model. The algorithm maintains a hierarchy of sphere coverings of the growth, supporting efficient random walks onto the growth by spherical moves. Anisotropy was introduced by restricting growth to certain preferred directions.

DOI: 10.1103/PhysRevE.72.031403 PACS number(s): 61.43.Hv

I. INTRODUCTION

The diffusion limited aggregation (DLA) [1] model has been the focus of a great deal of research due both to the fractal [2–4] and multifractal [5–7] properties of the clusters it produces, and to its underlying mathematical connection to diverse problems including solidification [8,9], viscous fingering [10], and electrodeposition [11,12]. Its key feature is that the surface irreversibly absorbs an incident diffusive flux, and growth velocity is locally proportional to that flux density.

The problem is mathematically ill-posed unless the growth is constrained to remain smooth below some "ultraviolet cutoff" length scale, which in most simulation studies has been supplied by a particle size or lattice scale. Experimentally the cutoff scale can be more subtle, for example in solidification regulated by surface tension it varies with the local incident flux density raised to power $-\frac{1}{2}$. Interest has also focused on the more general dielectric breakdown model [13] cases where growth velocity is proportional to the incident diffusive flux raised to some power η.

A feature of real solidification patterns is that they macroscopically strongly favor growth in specific directions, corresponding to microscopic crystal lattice directions. The tendency of snow crystals to grow six arms is well known, and lately this has been replicated in controlled laboratory studies [14]. Cubic crystalline anisotropy also produces striking anisotropic "dendrite" growth: succinonitryl is the classical example [15,16], and lately colloidal crystal exemplars have been observed in growth under microgravity [17,18].

The manner in which surface tension and its anisotropy select the morphology of growing tips has been the subject of intense analytical study [19]. Full numerical simulations of the continuum growth equations have confirmed the theory and extended the spatial range out to growths with significant side-branching [20,21], but none of these studies could claim to reach the asymptotic regime of fractal growth.

Simple lattice and particle-based simulations differ by having fixed cutoff scale and lacking realistic local detail, but they can reveal the limiting behavior of highly branched growth. In two dimensions, a range of different angular anisotropies has been shown to be relevant both by theory [22,23] and through simulations yielding self-similar dendritic morphologies. Our principal objective in this paper is to deliver the same level of understanding for three-dimensional simulations, which have not been systematically explored in the literature to date. In a paper to follow, we build on this to investigate what happens under the analogue of surface tension control [24].

We first introduce a new implementation of the DLA model that involves enclosing the aggregates with a series of coverings, each made up of a set of spheres, and show that it can successfully grow large, three-dimensional DLA clusters. This algorithm entails no intrinsic lattice or orientational bias, giving us a well-posed isotropic reference. It is the combination of this flexible new algorithm with advances in computing power which makes it feasible to study more than just the isotropic case of DLA in three dimensions.

We show how anisotropy can be introduced to the algorithm by confining growth to certain preferred directions, and combine this with a noise reduction technique in which growth is only permitted after $H \geqslant 1$ random walkers have hit a growth site on the cluster. We characterize growths using anisotropy functions which are sensitive to the growth of fingers along the possible favored directions. We present a systematic comparison of the evolution of growths within cubic symmetry, in particular the respective cases where growth is favored along the nearest-neighbor directions of one of the simple cubic, body-centered-cubic, and face-centered-cubic lattices. We also study growth with uniaxial bias, where growth in polar and planar directions is inequiva-

*Electronic address: N.R.Goold@warwick.ac.uk
†Electronic address: ellak@lorentz.leidenuniv.nl
‡Electronic address: r.c.ball@warwick.ac.uk

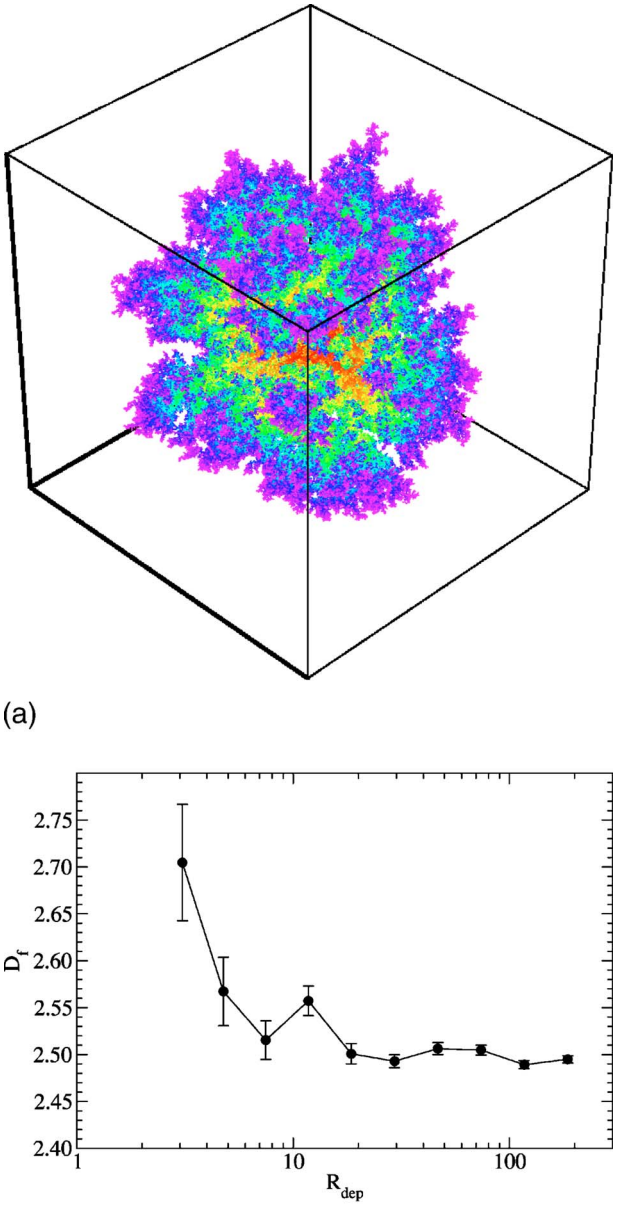

FIG. 1. (Color online) A three-dimensional DLA cluster grown using the new algorithm containing $N=10^6$ particles, and the fractal dimension D_f plotted against the deposition radius R_{dep} obtained by averaging over a sample of 100 such clusters. D_f converges to a value of ~ 2.5, in agreement with previous results.

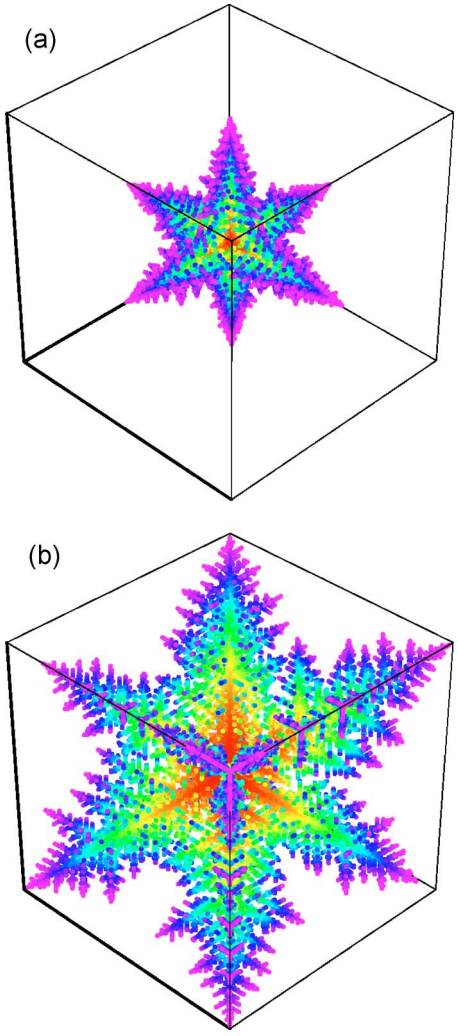

FIG. 2. (Color online) Anisotropic DLA clusters grown by the new method: (a) simple cubic case, and (b) body-centered cubic case. Each contains 3.16×10^4 sites, grown under noise reduction such that sites were grown after capturing $H=100$ walkers.

lently favored, particularly including the three-dimensional hexagonal lattice.

We show that sc and bcc aggregates approach universal, anisotropic asymptotic states independent of the level of noise reduction, and that the approach to each of these states follows a single mastercurve. fcc anisotropy is much slower to emerge, and we show that while high noise reduction clusters appear to approach an anisotropic fixed point in the same fashion, the existence of a different fixed point(s) for low noise reduction growths cannot be ruled out. For growth with uniaxial bias, we observe limiting polar-to-planar aspect ratios of the clusters which depend continuously on the level of input bias. Thus for the three-dimensional hexagonal lattice there appears to be a tunable continuum of asymptotic states.

II. GROWTH ALGORITHM

The original DLA model takes as its starting point a single fixed seed particle. A random walker is released from some distance away and diffuses freely until it hits the seed, at which point it sticks irreversibly. Further particles are released one at a time and a fractal cluster is formed. Early simulations were done on (mostly cubic) lattices, since this reduced the computer run-time required, and cluster sizes were limited to $N\simeq 10^4$ particles.

Modern DLA simulations are performed off-lattice and use a number of algorithmic tricks to speed up the growth, to which we describe a new contribution below. Since a diffusing particle should first approach the aggregate from a random direction, each new walker can be released from a randomly chosen point on a sphere that just encloses the cluster. When a walker is far from the cluster it is allowed to take

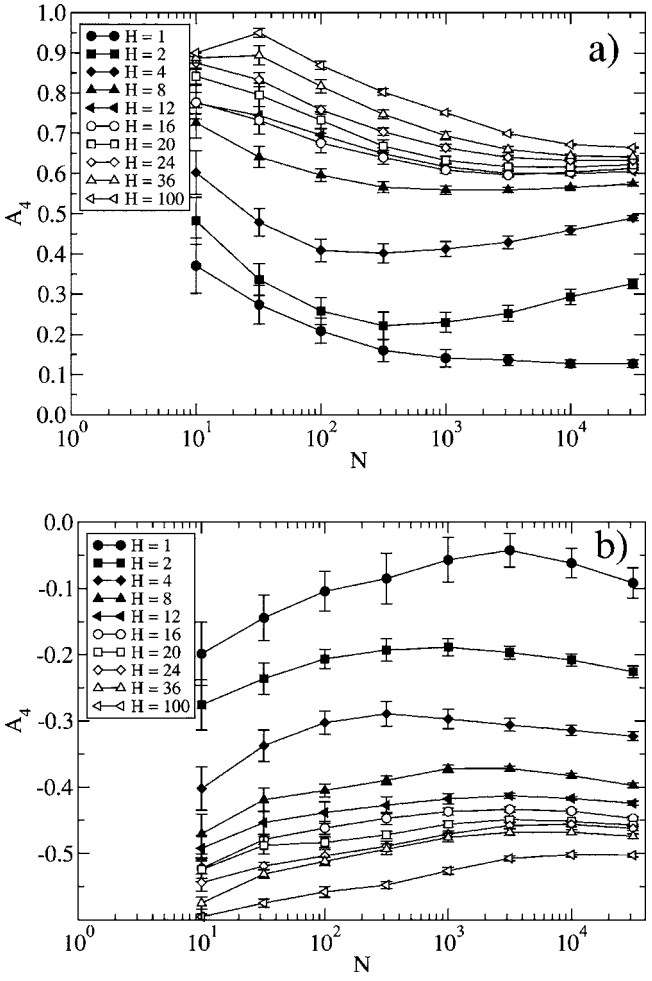

FIG. 3. Anisotropy function A_4 evaluated for (a) simple cubic and (b) body-centered cubic growths at various levels of noise reduction H as a function of the number of sites grown N. Each curve is based on the average over 10 clusters. Comparing to reference values in Table I, these confirm quantitatively the visual impression from Fig. 2 that the respective sc and bcc anisotropies are self-sustaining under growth.

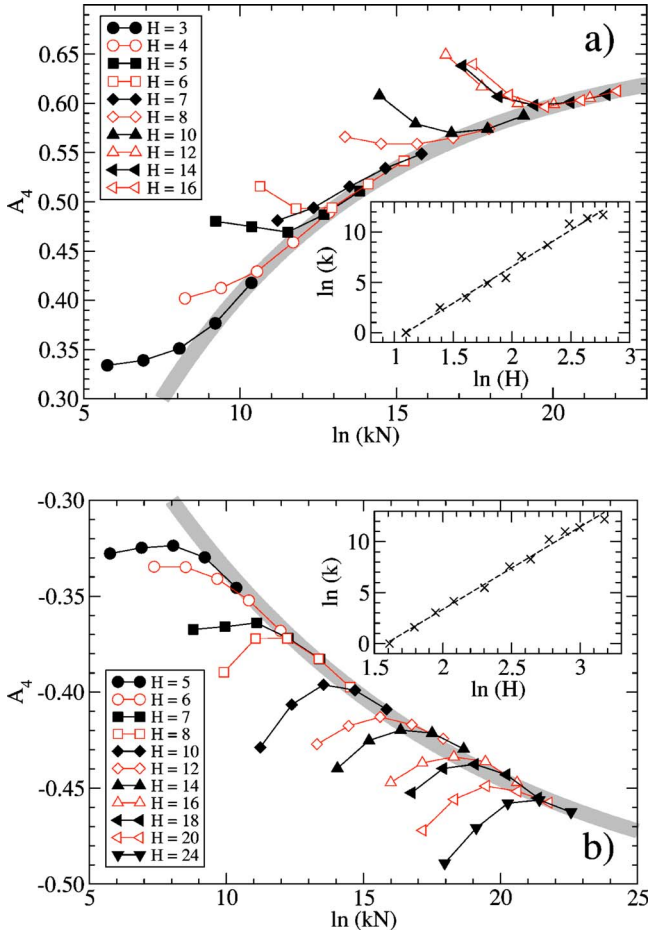

FIG. 4. (Color online) Mastercurves of the evolution of A_4 for (a) simple cubic and (b) body-centered cubic growths. These suggest a universal approach to respective sc and bcc fixed points. The gray curves are fits of the right tail of each mastercurve to a power-law correction to scaling form, for simple cubic $A_4(N,H)=0.66\{1+1.56[k(H)N]^{-0.14}\}$ and for bcc $A_4(N,H)=-0.52\{1+0.87[k(H)N]^{-0.09}\}$. The insets show how the shift factors $k(H)$ applied to N vary systematically with noise reduction parameter H.

larger steps than when it is nearby, as long as it never takes a step larger than its current distance to the nearest point of the cluster. A major development was the Brady-Ball algorithm [25], which involves covering the cluster with a series of coarse "mappings," to give a lower bound on the distance to the cluster without looking up the position of every cluster particle. A further refinement was invented by Tolman and Meakin [26], whereby the coarse mappings cover the cluster in a manner constrained to give a margin of safety: this enables much simpler (e.g., spherical) moves to be taken. Cluster sizes of $N \simeq 10^7$ are easily obtainable by these methods.

A. New data structure

Our new algorithm is a fundamentally off-lattice and dimension-independent development of the Brady-Ball-Tolman-Meakin algorithm. We represent the cluster in terms of a set of *zeroth level* spheres, and we maintain a hierarchy of coarser scale sphere coverings of these labeled by higher levels. For simplicity of exposition, we describe the case where the physical cluster particles are monodisperse, in which case it is convenient to choose the radius r_0 of the zeroth level spheres to correspond to the center-to-center distance between contacting particles ("sticking diameter").

Higher level coverings, $n>0$, each consist of a set of spheres of radius r_n such that every zeroth level sphere is *safely* covered, in the following sense: all points within distance ϕr_n of (the surface of) every zeroth level sphere lie inside the covering. Each covering is also *simply* contained by all higher level coverings. To make this structure easier to maintain, we further required that each zeroth level sphere was safely covered by a single (not necessarily unique) sphere at all levels $n>0$. We chose the coverings to have a geometric progression of size, with $r_n=\epsilon^{1-n}r_1$, and terminated the hierarchy when safe covering of the whole cluster was achieved by a single sphere.

TABLE I. Values of anisotropy functions A_4 and A_6 for growth along the nearest-neighbor directions of simple, body-centered, and face-centered-cubic lattices.

	Simple cubic	Body-centered cubic	Face-centered cubic
A_4	1	−2/3	−1/4
A_6	−8/13	−128/117	1

Each sphere at level $n>0$ carries a full set of *downlinks*. These consist of a pointer to every "child" sphere at level $n-1$ which overlaps the parent. In addition, we gave each sphere (below the highest level) one *uplink*, pointing to one of its parents; this is only required for the random walks (see later for choice).

B. Efficient random walks

The above construction is designed to support efficient moves for our random walkers. At each step we need only determine the highest level covering that the walker is outside to give a lower bound on the walker's distance from the cluster. This in turn entails tracking one (generally not unique) "enclosing" sphere which the walker does lie inside at the next level up.

Given that the walker lies inside an enclosing sphere at level m but outside the lower coverings, we first determine the nearest distance d from the walker to either the enclosing sphere or any of its children. The walker can then make a spherically distributed move of distance $d+\phi r_{m-1}$, because the nearest point of the cluster must be at least this far away.

After making the above move, we first check whether the walker is now outside the previous enclosing sphere: if so, we follow uplinks until we find a new enclosing sphere. We then recursively replace that sphere by any of its children which enclose the walker, until a lowest level enclosing

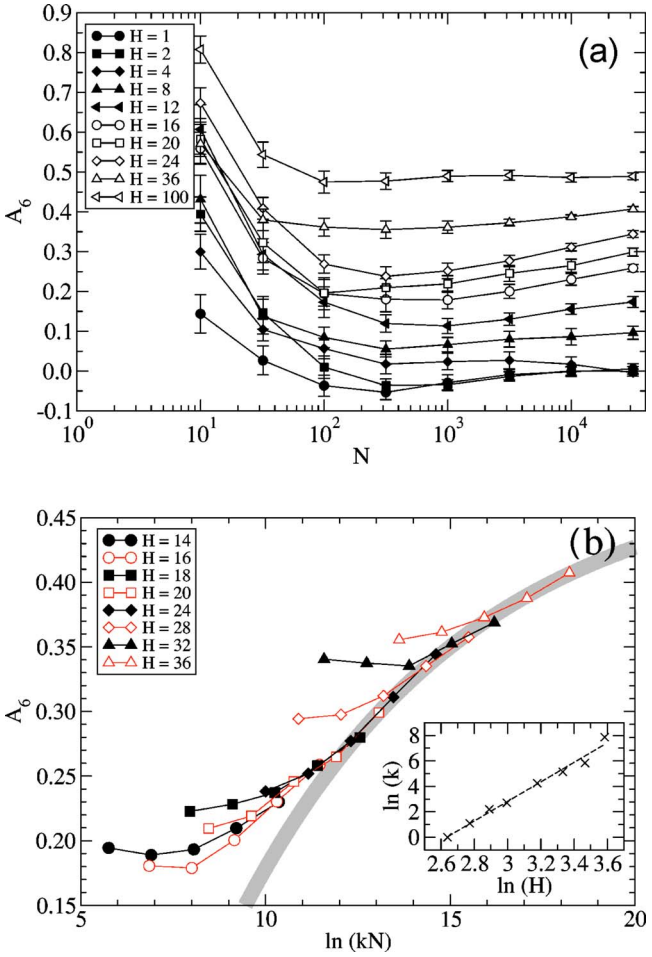

FIG. 5. (Color online) (a) Anisotropy function A_6 evaluated for fcc growths, based on the average over 10 clusters per curve. Only at higher noise reduction levels is there a clear indication that the fcc anisotropy is sustained under growth. (b) Mastercurve for fcc growths at $H\geqslant 14$, which do appear to exhibit a common evolution, with the corresponding shift factors inset. The gray curve is a fit of the right tail to power-law correction to scaling form, $A_6(N,H)=0.49\{1+3.15[k(H)N]^{-0.16}\}$.

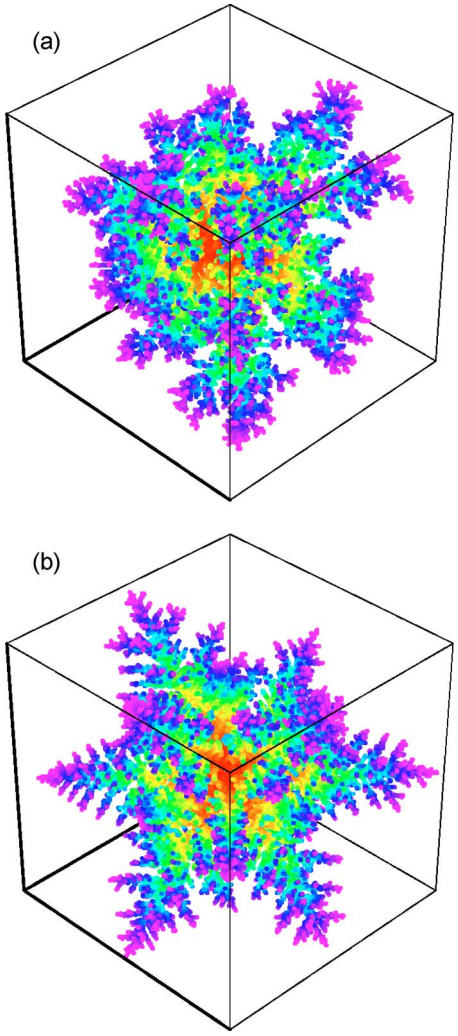

FIG. 6. (Color online) fcc clusters grown by the new method: (a) low noise reduction $H=6$, and (b) high noise reduction $H=100$. Both clusters contain 3.16×10^4 sites grown. The low noise reduction case appears to show some growth bias to the bcc lattice directions (corners) as per bcc lattice growth in Fig. 2. The high noise reduction cluster exhibits growth in all 12 fcc lattice directions, which correspond to the mid-edges of the box drawn.

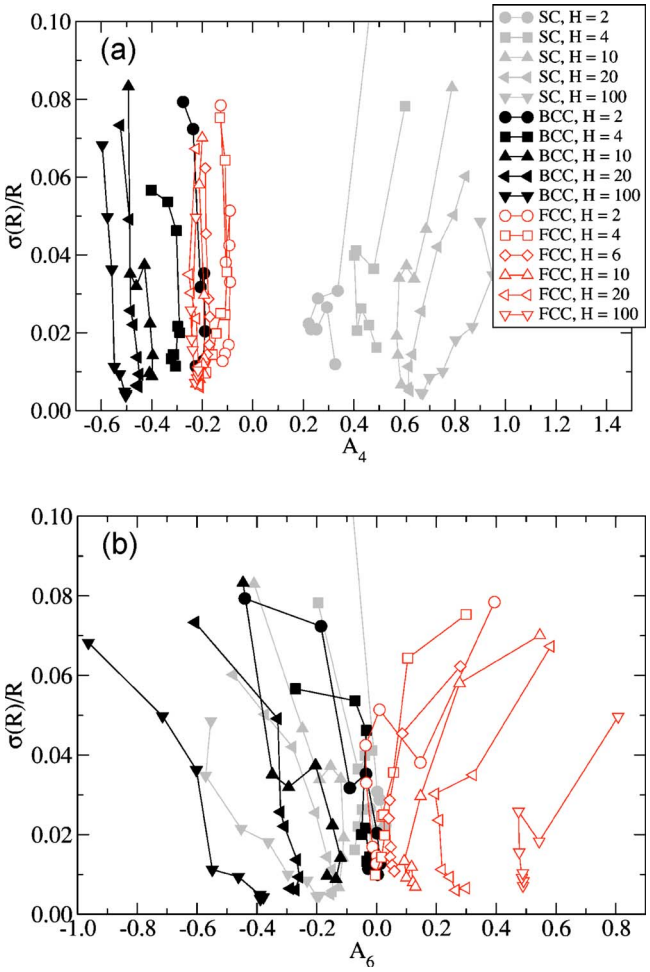

FIG. 7. (Color online) The relative fluctuation in cluster radius (at fixed N), plotted against each of the anisotropy measures A_4 and A_6 as clusters grow. Increasing N corresponds to moving generally downwards in these plots, and the symbols are the same on both panels.

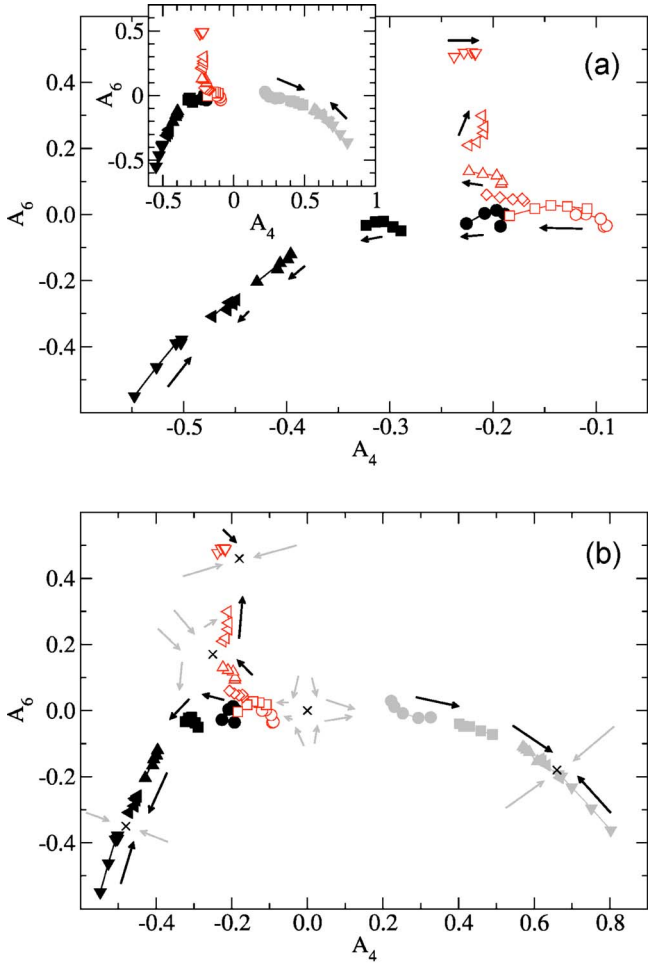

FIG. 8. (Color online) (a) The evolution of clusters in the plane of A_4 and A_6 for bcc and fcc clusters at various noise reduction levels (always averaging over samples of 10), with arrows to indicate the direction of trajectories. The inset shows the well separated evolution of sc clusters in the same plane. (b) The same data can be interpreted as renormalization flows for how effective parameters evolve as a function of length scale, leading to the inferred fixed points shown (crosses). It is an assumption here that the lowest relevant angular harmonics A_4,A_6 do capture the key distinction between the three different applied anisotropies. Bold arrows show observed evolution whereas gray arrows show the presumed flow from other starting points. The symbols on both panels are the same as those in Fig. 7.

sphere is found again as required for the next move of the walker.

To ensure that walkers can ever actually hit the cluster, we impose a very small *minimum* move distance, typically $10^{-3}r_0$, when the calculated nearest distance to the cluster is less than this. Walkers are deemed to have hit the cluster when they thereby land inside a cluster particle. For standard off-lattice DLA growth, they are then "backed up" to the cluster perimeter (by linear interpolation of trajectory) and added to the cluster.

C. Data update and constraints

When each new particle is added to the cluster, we must assure that they are safely covered at each level $n>0$. We start at the maximum level, and create new maximum levels above it if required. Then we move down levels to $n=1$ checking for safe coverage at each, noting the sphere that provided this. A level n sphere that safely covers our new site will necessarily overlap that which did so at the previous level $n+1$, so the search at each level can be restricted to the children of the previous safe container. If none of these give safe coverage, we must add a new sphere at level n, ensuring that the integrity of the data structure is maintained and all the required new links are put in place.

The safe container at level $n+1$ is made the parent of the new sphere at level n; this is the uplink used by our random walkers. The new sphere could simply be centered on the particle we wish to add; however, in an attempt to maximize the efficiency of our coverings, we offset the new sphere by a distance γr_n in the direction of local growth. This offset is constrained by our safe coverage requirement to obey $r_0+\gamma r_n+\phi r_n<r_n$, which is most severe for $n=1$ leading to

$$r_1(1-\gamma-\phi)>r_0. \tag{1}$$

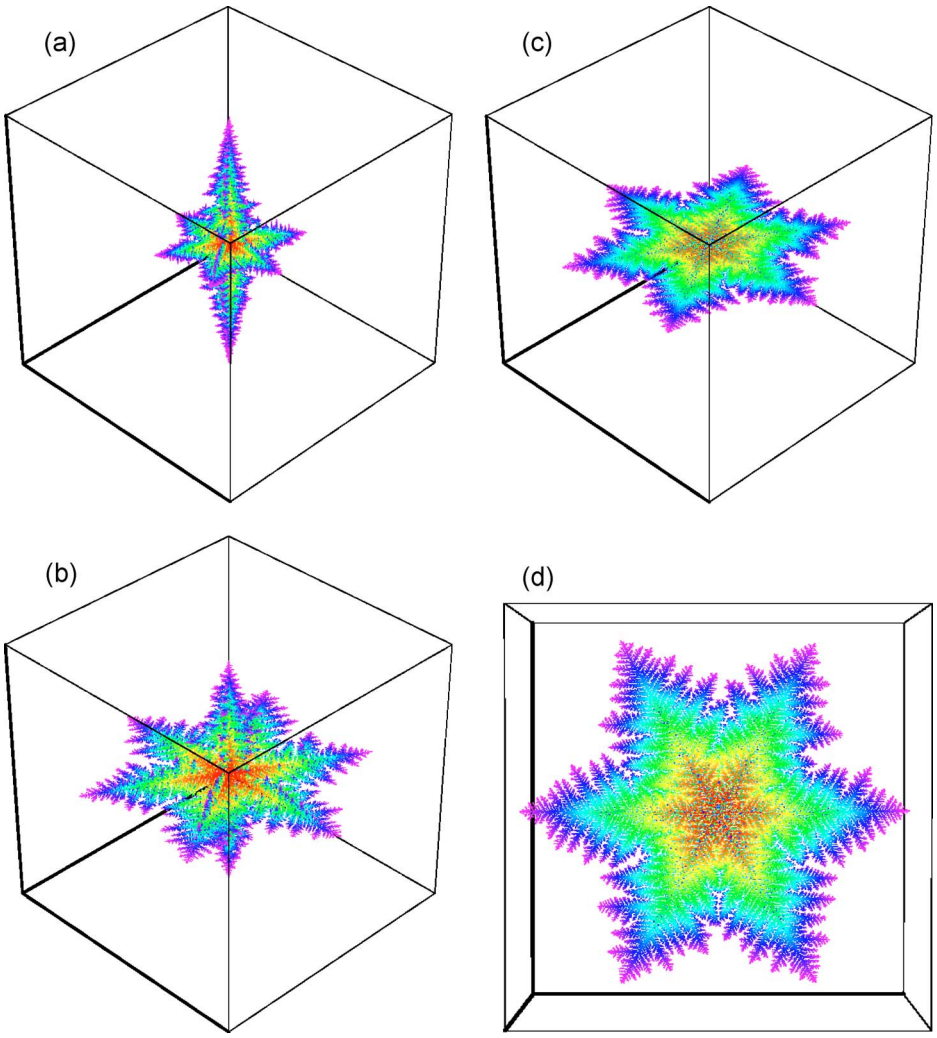

FIG. 9. (Color online) Clusters grown favoring six planar directions and two polar directions. The parameter p is a measure of the relative ease of planar growth compared with polar, with high values of p favoring planar growth. Shown are (a) $p=1$, (b) $p=1.5$, and (c) $p=4$; (d) shows the $p=4$ cluster viewed from above, highlighting the complex six-armed morphology of these growths.

We must now find all the spheres which may need a downlink to or from the new sphere. To facilitate this, we impose that each level covering is simply (but with no required margin) contained within those above it. In terms of our parameters, this requires $r_n(1+\gamma) < \phi r_{n+1} + r_0$, and choosing a geometric progression of radii $r_n = r_1/\epsilon^{n-1}$ with $\epsilon < 1$ and no limit on n then requires

$$1 + \gamma < \frac{\phi}{\epsilon}. \tag{2}$$

This constraint ensures that our new sphere is completely covered by the level $n+2$ safe container, whose child list will hence contain all the level $n+1$ spheres that need linking to the new sphere. Similarly, our new sphere is also covered by the level $n+1$ safe container, and so any level $n-1$ spheres to which the new sphere needs downlinks are guaranteed to be children *of the children* of that safe container. Thus by remembering the spheres which provided safe coverage at the previous two levels and selecting parameter values subject to the constraints (1) and (2), we can insert all the necessary new links, and ensure the integrity of our data structure remains intact as the cluster growth proceeds.

D. Parameter optimization and standard off-lattice results

Taking $r_0=1$ for convenience, a somewhat ad hoc optimization scheme suggested the following parameters to minimize the run-time of our program in three dimensions: $r_1=2.1$, $\gamma=0.29$, $\phi=0.4$, and $\epsilon=0.3$. We observe that the order of the algorithm is close to linear in N, consistent with the earlier discussion of Ball and Brady [25]. Figure 1 shows a large off-lattice DLA cluster grown in three dimensions by the new scheme and the convergence of measured fractal dimension D_f to a value ~ 2.5, in good agreement with previous simulations [26,27].

In terms of absolute computational performance, our algorithm which is dimension-independent comes, in two dimensions, within a factor of 2 of the speed of the code used in Ref. [2] which is two-dimensionally specific. So far as we know, the latter is the most efficient descendent of the Ball-Brady-Meakin-Tolman codes.

III. ANISOTROPY AND NOISE REDUCTION

We introduce anisotropy to our simulations by restricting growth to a set of preferred directions, effectively growing our clusters on a lattice. To this end, we changed the local relationship between walker capture and cluster growth, so

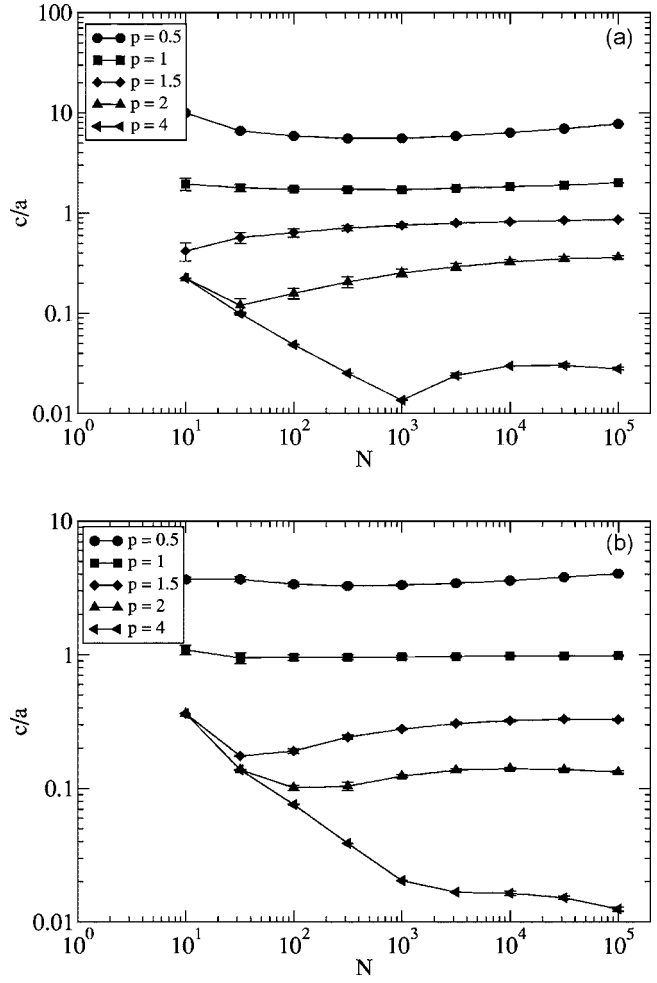

FIG. 10. Aspect ratios of (a) hexagonal growths and (b) sc growths, both with tunable input polar anisotropy p. The data are from five clusters of each type for each value of p; using both polar arms and the six (hexagonal) or four (sc) planar arms means each cluster provides 12 or 8 measurements, respectively, of an aspect ratio at size N.

that each zeroth level sphere was a site of walker capture. Only when such a "sticky site" had captured a set threshold number of walkers H was growth implemented, and this growth consisted of new sticky sites offset in each of the (ungrown) lattice directions.

Requiring $H>1$ walkers for growth gives better averaging over the diffusion field, amounting to a noise reduction. Noise reduction has been widely used for on-lattice planar DLA simulations [28], where it was found to considerably accelerate the approach to asymptotic morphology. We exploit it both for that reason and as a probe of universality by the concordance of asymptotic behavior between growths at different H.

A. Cubic symmetry lattices

We have first grown aggregates favoring growth in the local simple, body-centered, and face-centered cubic lattice directions, which are relatively straightforward in having all their nearest-neighbor directions geometrically equivalent. To characterize the macroscopic anisotropy of these cubic symmetry lattice growths, we use functions

$$A_K = \frac{1}{N}\sum_{i=1}^{N} a_K(x_i,y_i,z_i),$$

where (x_i,y_i,z_i) are the coordinates of the ith of N particles relative to the seed of the growth, and a_K are functions with cubic symmetry constructed out of angular harmonics of order K, with minimal order to distinguish the different lattice responses of study.

Growth biased toward the direction of simple cubic axes (relative to the cluster seed) is signaled by a positive average to the following harmonic of order 4:

$$a_4 = \frac{5}{2r^4}(x^4+y^4+z^4) - \frac{3}{2},$$

where $r^2=x^2+y^2+z^2$ and the normalization is chosen such that $A_4=1$ for growth exactly along the lattice axes. Likewise, growth along the nearest-neighbor directions of an fcc lattice gives $A_6=1$ based on

$$a_6 = \frac{112}{13r^6}\left(x^6+y^6+z^6+\frac{15}{4}(x^4y^2+x^2y^4+x^4z^2 + x^2z^4+y^4z^2+y^2z^4)\right) - \frac{120}{13}.$$

The combination of these two enables us to distinguish by sign growth along sc, bcc, or fcc directions as summarized in Table I, where values given are for the extreme case of growth confined to the corresponding nearest-neighbor directions from the central seed.

B. Lattices with planar-polar bias

Lattices where the natural growth directions are geometrically inequivalent present a greater challenge, because there is then no natural equivalence to the corresponding local growth rules. We have focused here on the hexagonal prismatic lattice with six equivalent planar directions and two polar directions of growth. Because the polar directions are inequivalent (by any symmetry) to the planar ones, we were naturally led to explore growth with different values of H in the two classes of direction, with

$$H_z = pH_{xy}.$$

The physical significance of p is that it globally biases the ratio of local growth velocities in the two classes of direction. We also explore the corresponding planar-polar bias imposed on simple cubic lattice clusters as a reference.

We found the clearest characterization of the corresponding growth response of these clusters simply by measuring their aspect ratios, which we calculate using extremal radii in each lattice direction, that is, c/a in terms of crystallographic notation.

IV. CUBIC SYMMETRY RESULTS

We grew aggregates favoring sc, bcc, and fcc lattice directions at several levels of noise reduction H from 1 to 100,

and measured their response using our anisotropy functions A_K. The clusters were grown to size $N=3.16\times10^4$ particles, where a site was included in this tally only when it had been hit H times.

Figure 2 shows an example sc and bcc clusters grown at the highest level of noise reduction $H=100$. Both clusters have major arms in the appropriate lattice directions, and each arm exhibits secondary growth along the remaining favored directions.

The measured anisotropy A_4 for sc and bcc growths at various H is shown in Fig. 3. Both sets of clusters appear to approach universal asymptotic values of A_4 independent of noise reduction: $A_4(\infty)\simeq0.66\pm0.02$ for sc growths and $A_4(\infty)\simeq-0.52\pm0.02$ for bcc growths. These values can be approached from both above and below, depending on H.

The consistency of the shapes of the anisotropy curves suggests that for these types of growth there may exist universal late stage evolution of A_4 toward its asymptotic value, as a function of rescaled N. To test this hypothesis, for each value of H we shifted the curve along the N axis by a factor $k(H)$ until, by eye, they appeared to follow a single master curve. Figures 4(a) and 4(b) show the success of this procedure for both the sc and bcc growths. For each case, we have used only the results for $N>10^2$ in order to be sure of the correct general trend, and we could not use the very low H curves because they vary too little across the simulation range to give sufficient vertical overlap. The figure shows simple power-law relationships between the noise reduction H and the shift factors $k(H)$ in both cases, further evidence that a coherent universal scaling underlies the asymptotic evolution of sc and bcc growths.

In the sc case, Fig. 4(a), the shifted curves for values of H from 3 to 16 are shown. The interpretation of this coherent behavior corresponding to a single dominant asymptotic correction to scaling suggests the fitted form shown,

$$A_4(N,H)=A_4(\infty)\{1+a[k(H)N]^{-\nu}\}.$$

Our estimate is that $\nu_{sc}=0.14\pm0.02$. For $H>16$, the anisotropy curves lie close to the asymptotic value of A_4 and are rather flat, so the curve-shifting process fails. The curves for very high values $H\geqslant28$ are increasingly dominated by the earlier regime of steeper approach to the asymptotic value from above, which is beyond the master curve and presumably corresponds to a different correction to scaling.

For the bcc case, Fig. 4(b), the anisotropy is much slower to emerge from the noise and the curves for all values of H except the very highest $H=100$ approach the asymptotic value from the same direction, and the mastercurve includes all values of H from 5 to 24. We estimate that the correction to scaling exponent governing the asymptotic approach of A_4 is given in this case by $\nu_{bcc}=0.09\pm0.04$. Above $H=24$, the mastercurve procedure for bcc degenerates in the same fashion as the sc case at large H.

Anisotropy curves A_6 for fcc growths are shown in Fig. 5(a), and it is immediately apparent that their behavior is not as straightforward as the sc and bcc cases. For high H growths, A_6 appears to be increasing in a fashion similar to that previously observed, suggesting the existence of a fixed point of anisotropy for fcc growth at $A_6(\infty)\simeq0.49\pm0.02$. All the curves approach this value from below, suggesting that the fcc anisotropy is much slower to emerge from the noise than the sc and bcc anisotropies. This seems reasonable given that the fcc anisotropy has significantly more competing growth directions than the other growths, and we have verified that the $H=100$ clusters do indeed appear to have a full set of 12 arms [see Fig. 6(b)]. A mastercurve for these higher values of H is shown in Fig. 5(b), and seems to describe these results fairly well with a correction to scaling exponent $\nu_{fcc}=0.16\pm0.06$.

For low noise reduction clusters $H<8$, however, A_6 does not increase over the course of the growth, and if anything appears to be *decreasing* at large N toward a value of about zero, suggesting the possible existence of another fixed point. Visualizations of these low H fcc clusters appeared to indicate some growth along the bcc lattice directions; Fig. 6 shows an example of this for a low noise reduction $H=6$ cluster, and for comparison a high noise reduction $H=100$ cluster exhibiting some growth in all 12 fcc lattice directions.

We were hence led to apply the bcc anisotropy function A_4 to the fcc aggregates, and for comparison A_6 was also evaluated for the bcc and sc clusters. Studies of two-dimensional anisotropic DLA [29] have had some success focusing on the interplay between anisotropy and noise in the growth process, and in this spirit we measured $\sigma(R)/R$, where R is the deposition radius of a cluster and $\sigma(R)$ is the standard deviation of this measurement. This quantity offers a simple measure of fluctuations due to noise during cluster growth; $\sigma(R)/R$ is plotted against A_4 in Fig. 7(a) and against A_6 in Fig. 7(b) for clusters of each type at various H.

Figure 7(a) shows that for all clusters, the noise decreases reasonably monotonically as growth proceeds. sc and bcc growths for all H can be seen to converge toward their respective fixed-point values for A_4 of approximately 0.66 (sc) and −0.52 (bcc). The fcc growths are all grouped around $A_4\simeq-0.2$, and this plot fails to explain the behavior of the low H fcc clusters. However, Fig. 7(b) gives us an idea of what may be happening: whereas the higher H growths head toward the same final value ($A_6\simeq0.49$), the curves for the low H fcc clusters have not turned toward this value and appear to be following similar trajectories to the low H bcc clusters. All the sc and bcc clusters appear to be approaching common asymptotic values of A_6 of approximately −0.2 and −0.35, respectively.

Further evidence for this explanation of the fcc cluster behavior is given by plotting A_4 against A_6 for bcc and fcc growths in Fig. 8(a). This clearly shows the bcc clusters evolving (in a direction dependent on H) toward a fixed point. The high H fcc growths also head to their own fixed point, whereas the low H growths are moving in a different direction, toward the bcc fixed point. The inset of Fig. 8(a) shows the position of the sc growths in the A_4,A_6 plane; they can also be seen to approach a fixed point from different directions depending on H.

This information allows us to build what we believe to be a consistent picture of the evolution of all three types of growth, interpreted in terms of how the parameters A_4 and A_6

evolve as a function of increasing lengthscale. This is shown in Fig. 8(b). Our anisotropy curves have shown the existence of stable fixed points, for each of sc, bcc, and high noise reduction fcc clusters: assuming that the variables A_4 and A_6 capture the key distinction between the different anisotropies studied, these directly imply the three separate stable fixed points shown in Fig. 8(b). There should by symmetry be a fixed point located at (0, 0) in the A_4, A_6 plane corresponding to isotropic growth, and it must have one unstable direction driving the separation of evolution between sc and the other clusters. The differing trajectories of the fcc clusters dependent on H imply the existence of another fixed point, with unstable direction separating the flow of low H fcc clusters following bcc from the flow of high H fcc clusters toward their own fixed point. The remaining directions in the A_4, A_6 plane associated with all these fixed points we infer to be stable because of how strongly the simulations at different H conform to common curves rather than filling the plane. The scheme of fixed points shown in Fig. 8(b) is thus the simplest compatible with all the data, and amounts to a qualitative prediction of the ultimate fate of growths from any transient combination of A_4 and A_6.

While selected clusters could be grown a decade larger, we do not believe it likely that the ultimate behavior of low noise reduction fcc will be readily clarified by brute force in this way. Real space renormalization group methods such as developed in Ref. [29] may contribute given some ansatz to coarse grain the anisotropy measures; however, our data in Fig. 7 suggest that the fixed points may be at inconveniently large renormalized values of noise reduction, $H \geqslant 10^4$.

V. PLANAR-POLAR ASYMMETRY

We next turn our attention to growth on the hexagonal prismatic lattice and the analogous polar-planar anisotropy imposed on simple cubic lattice growth. For economy of computation, we fixed the value $H_{xy}=100$ for growth in the locally planar directions and then varied the corresponding value for locally polar growth through $H_z=pH_{xy}$ with values of p ranging from 0.5 to 4. The lowest values of p produce columnlike growths while the highest resulted in virtually flat aggregates, and example clusters from the hexagonal prismatic lattice are shown in Fig. 9.

Measured aspect ratios of the hexagonal clusters are shown in Fig. 10(a) and exhibit puzzling trends. The results are from five clusters of size $N=10^5$ (sites grown) at each value of p, although since a cluster possesses six planar and two polar arms each provides us with effectively 12 measurements of an aspect ratio. Strikingly, the aspect ratios remain almost constant for $N \geqslant 10^3$, that is, for two orders of magnitude, at values tunable by selection of p.

To investigate this interesting result further, we tuned the polar growth of some sc clusters in the same way. Since these clusters possess fewer competing arms than the hexagonal growths, for the same size N we might expect that they should be more converged toward their asymptotic states. The aspect ratios of these clusters are shown in Fig. 10(b), and they appear very similar to the hexagonal results.

The behavior of aspect ratios at intermediate p is surprising. The simplest expectation would have been that the observed behavior at extreme p corresponded to two stable fixed points with $c/a \to 0, \infty$ respectively. These should then most simply be separated by a single fixed point at finite c/a, unstable with respect to variations in p in the sense that our plots of aspect ratio versus N for different p should diverge around it. In the cubic case, any such single intermediate fixed point would, by symmetry, have to be at $p^*=1$.

Our results are more compatible with the existence of a continuous spectrum of fixed points at intermediate aspect ratio, which depend directly on the input anisotropy. Under this scenario, the input anisotropy (presumably in combination with other microscopic parameters) remains relevant to the fixed point. One can still then have breakaway to simpler fixed points at extreme values of p, as we appear to see for $p=0.5$ and $p=4$, if the fixed point stability is sensitive to the input parameters.

VI. CONCLUSIONS

Our dimension-independent numerical implementation of the DLA model has enabled us to explore the effects of a range of lattice anisotropies on three-dimensional diffusion limited aggregates, leading to a mixture of expected and unexpected results. As in two dimensions, noise reduction proves a crucial aid toward asymptotic behavior.

For cubic anisotropies, the two lowest-order relevant angular harmonic amplitudes, A_4 and A_6, appear jointly to provide an effective probe of the cluster evolution. Simple cubic and bcc growths then behave simply, approaching universal trajectories as evidenced by our mastercurves, toward respective simple fixed points in the A_4, A_6 plane.

Face-centered-cubic anisotropy is subtle. High noise reduction clusters appear to approach a common asymptotic state, distinct from but analogous to those found for sc and bcc. By contrast fcc growths at lower noise reduction appear to evolve toward the bcc fixed point, although the final appearance of these clusters remains an open question. The minimal interpretation of all the observed sc, bcc, and fcc growth as a flow in the A_4, A_6 plane involves at least five fixed points.

For hexagonal anisotropy in three dimensions, the key challenge presented is the inequivalence of planar and polar directions. The simple positive result is that moderate favoring of planar growth locally coupled to three-dimensional diffusion controlled growth does lead to clusters with markedly planar morphology. This confirms a possible mechanism behind near-planarity of snow crystals.

The apparently tunable and stable aspect ratios of clusters at intermediate input polar-planar anisotropy are an unexpected surprise. It appears robust in that both hexagonal and cubic cases showed this behavior. At face value it suggests fixed points depending continuously on some asymptotically relevant combination of input anisotropy parameters, which prompts a theoretical framework in which to model this.

This paper leaves unresolved the ultimate behavior of low noise reduction fcc or the apparently tunable polar-planar anisotropy of hexagonal clusters. We do not expect that extra

numerical efforts would be decisive; instead, one is tempted to turn to real space renormalization group techniques (see, e.g., Ref. [29])—though technical difficulties, such as very large values of the renormalized noise reduction, hinder progress there. These issues seem ripe to benefit from new theoretical ideas.

ACKNOWLEDGMENTS

This research has been supported by the EC under Contract No. HPMF-CT-2000-00800. NRG was supported by an EPSRC CASE award. The computing facilities were provided by the Centre for Scientific Computing of the University of Warwick, with support from the JREI.

[1] T. A. Witten and L. M. Sander, Phys. Rev. Lett. **47**, 1400 (1981).
[2] E. Somfai, L. M. Sander, and R. C. Ball, Phys. Rev. Lett. **83**, 5523 (1999).
[3] M. Plischke and Z. Rácz, Phys. Rev. Lett. **53**, 415 (1984).
[4] A. Coniglio and M. Zannetti, Physica A **163**, 325 (1990).
[5] C. Amitrano, Phys. Rev. A **39**, 6618 (1989).
[6] M. H. Jensen, J. Mathiesen, and I. Procaccia, Phys. Rev. E **67**, 042402 (2003).
[7] E. Somfai, N. R. Goold, R. C. Ball, J. P. DeVita, and L. M. Sander, Phys. Rev. E **70**, 051403 (2004).
[8] J. S. Langer, Rev. Mod. Phys. **52**, 1 (1980).
[9] W. W. Mullins and R. F. Sekerka, J. Appl. Phys. **34**, 323 (1963).
[10] J. Nittmann, G. Daccord, and H. E. Stanley, Nature (London) **314**, 141 (1985).
[11] M. Matsushita, M. Sano, Y. Hayakawa, H. Honjo, and Y. Sawada, Phys. Rev. Lett. **53**, 286 (1984).
[12] R. M. Brady and R. C. Ball, Nature (London) **309**, 225 (1984).
[13] L. Niemeyer, L. Pietronero, and H. J. Wiesmann, Phys. Rev. Lett. **52**, 1033 (1984).
[14] K. G. Libbrecht and V. M. Tanusheva, Phys. Rev. E **59**, 3253 (1999).
[15] S. C. Huang and M. E. Glicksman, Acta Metall. **29**, 717 (1981).
[16] D. P. Corrigan, M. B. Koss, J. C. LaCombe, K. D. de Jager, L. A. Tennenhouse, and M. E. Glicksman, Phys. Rev. E **60**, 7217 (1999).
[17] W. B. Russel, P. M. Chaikin, J. Zhu, M. V. Meyer, and R. Rogers, Langmuir **13**, 3871 (1997).
[18] J. Zhu, M. Li, R. Rogers, W. Meyer, R. H. Ottewill, W. B. Russel, and P. M. Chaikin, Nature (London) **387**, 883 (1997).
[19] M. E. Glicksman and S. P. Marsh, in *Handbook of Crystal Growth*, edited by D. T. J. Hurle (Elsevier, Amsterdam, 1993), p. 1077.
[20] W. L. George and J. A. Warren, J. Comput. Phys. **177**, 264 (2002).
[21] R. Kobayashi, Physica D **63**, 410 (1993).
[22] P. Meakin, Phys. Rev. A **36**, 332 (1987).
[23] R. C. Ball, R. M. Brady, G. Rossi, and B. R. Thompson, Phys. Rev. Lett. **55**, 1406 (1985).
[24] N. R. Goold, E. Somfai, and R. C. Ball (unpublished).
[25] R. C. Ball and R. M. Brady, J. Phys. A **18**, L809 (1985).
[26] S. Tolman and P. Meakin, Phys. Rev. A **40**, 428 (1989).
[27] N. E. Bowler and R. C. Ball, Phys. Rev. E **71**, 011403 (2005).
[28] R. C. Ball, N. E. Bowler, L. M. Sander, and E. Somfai, Phys. Rev. E **66**, 026109 (2002).
[29] P. W. Barker and R. C. Ball, Phys. Rev. A **42**, 6289 (1990).